RSC Advances

PAPER

Cite this: *RSC Adv.*, 2019, **9**, 38047

Improved light-harvesting and suppressed charge recombination by introduction of a nanograss-like SnO_2 interlayer for efficient CdS quantum dot sensitized solar cells†

Sangaraju Sambasivam,[a] Chandu V. V. Muralee Gopi,[b] Hee-Je Kim[b] and Ihab M. Obaidat*[a]

Received 10th October 2019
Accepted 15th November 2019

DOI: 10.1039/c9ra08234d

rsc.li/rsc-advances

Quantum dot sensitized solar cell (QDSSC) performance is primarily limited by the recombination of charges at the interfaces of TiO_2/quantum dot (QD) sensitizer/electrolyte. Hence, blocking or suppressing the charge recombination is an essential requirement to elevate the QDSSC performance to the next level. To retard the charge recombination, herein, we propose the introduction of a SnO_2 nanograss (NG) interlayer on the surface of TiO_2 using the facile chemical bath deposition method. The SnO_2 NG interlayer not only inhibits the interfacial recombination processes in QDSSCs but also enhances the light-harvesting capability in generating more excitons. Hence, the TiO_2/SnO_2 NG/CdS QDSSCs can achieve the power conversion efficiency of 3.15%, which is superior to that of a TiO_2/CdS device (2.16%). Electrochemical impedance spectroscopy, open-circuit voltage decay and dark current analyses confirm that the recombination of charges at the photoanode/electrolyte interface is suppressed and the life time is improved by introducing the SnO_2 NG interlayer between the TiO_2 and CdS QD sensitizer.

1. Introduction

Because of the increased environmental pollution and the limited fossil fuels, the demand for renewable and sustainable energy systems, such as solar energy, has increased over the last few decades. Among the different solar energy systems, third-generation solar cells such as quantum dot sensitized solar cells (QDSSCs) are gaining considerable interest owing to their advantages of inorganic structure, high theoretical efficiency, easy fabrication and low-cost.[1,2] Various metal chalcogenide-semiconductors such as CdS, CdSe, PbS, $CdSe_xS_{1-x}$, $CuInS_2$, CuInZnS, *etc.* have been investigated as promising sensitizers for the QDSSCs due to their tunable band gap, high absorption coefficient and multiple exciton generation (MEG).[3–5] A typical structure of the QDSSC is composed of a QD-sensitized TiO_2 photoelectrode, polysulfide electrolyte (S^{2-}/S_n^{2-}), and counter electrode, which leads to various hetero-interfaces.[6–8] Although QDs have unique characteristics, the QDSSCs achieved a low power conversion efficiency (PCE = 12%) due to the recombination of charges that occur at the photoanode/QDs/electrolyte interfaces.[9,10] Hence, considerable attempts have been carried out to suppress the charge recombination, such as the use of a passivation layer on QDs surface, the introduction of metal doping in QDs, and overcoating wide band gap (or insulating) materials over TiO_2 surface or QDs, which results in the enhanced QDSSCs performance.[11–13]

Recently, Z. Ren *et al.* reported that the application of amorphous TiO_2 intermediate layer between the interface of QDs and ZnS/SiO_2 layer, effectively suppressed the charge recombination and improved the photovoltaic performance.[13] Recently, Li *et al.* developed the effective integration of ultra-high density well-separated ZnO nanocrystals (NCs) homo-epitaxially grown on the surface of an individual vertically oriented single-crystalline (SC) ZnO nanoneedle (NN).[14] The fabricated monolithic ZnO NCs-on-NN SC hybrids may hold great promise for enhanced photovoltaic performance (*e.g.*, electron mobility) of ZnO NC-sensitized solar cells. Very recently, Y. S. Lee *et al.* introduced the TiO_2/ZnS/CdS/ZnS cascade structure, in which the presence of ZnS intermediate layers are not only capable of retarding the charge recombination but also improve the light-harvesting efficiency, resulting in the enhanced power conversion efficiency (3.69%).[15] Z. Du *et al.* studied the CdSe QDSSCs based on FTO/TiO_2 without and with $TiCl_4$ treatment.[16] The QDSSCs based on FTO/TiO_2/$TiCl_4$/CdSe photoanode exhibited higher PCE (5.36%) than the FTO/TiO_2/CdSe (5.11%), which is mainly due to the $TiCl_4$ treatment

[a]*Department of Physics, United Arab Emirates University, Al-Ain 15551, United Arab Emirates. E-mail: iobaidat@uaeu.ac.ae*

[b]*Department of Electrical Engineering, Pusan National University, Geumjeong-gu, Busan, South Korea-46241. E-mail: naga5673@gmail.com; heeje@pusan.ac.kr*

† Electronic supplementary information (ESI) available. See DOI: 10.1039/c9ra08234d

that reduced the recombination of charges at the interface of TiO_2 and CdSe QDs. Very recently, Ozu *et al.* reported ZnO nanowire (NW) passivation by an ultrathin SnO_2 layer, reducing the density of the deep traps by the absorbed oxygen and hydroxyl groups on the ZnO NW surface.[17] SnO_2 passivation not only reduced the surface recombination but also led to an upward shift of the Fermi energy, causing more efficient electron transfer to ZnO. Very recently, E. N. Jayaweera *et al.* developed the SnO_2/MgO films for the CdS/ZnS based QDSSCs (SnO_2/MgO/CdS/ZnS) to boost the solar cell performance by efficiently preventing the charge recombination at the interface of SnO_2/sensitizer.[18] As a result, the SnO_2/MgO/CdS/ZnS QDSSC achieved a PCE of 1.33%. Therefore, the idea of deposition of wide band-gap semiconductor materials on the surface of semiconductor nanoparticles could effectively improve the QDSSC performance.

Motivated from the recent results of hindering the charge recombination at the TiO_2/QDs/electrolyte interfaces, herein, we propose the introduction of a novel SnO_2 nanograss (NG) interlayer on TiO_2 surface *via* a simple chemical bath deposition (CBD) route. The deposition of SnO_2 NG between the TiO_2 and CdS QDs suppresses charge recombination, resulting in enhanced QDSSC performance. Further, the photoanode of TiO_2/SnO_2 NG/CdS achieves improved light-harvesting and also provides efficient charge transport. The QDSSCs based on TiO_2/SnO_2 NG/CdS photoelectrode showed an impressive PCE of 3.15% under one sun illumination, which was much higher than that with TiO_2/CdS photoelectrode (2.16%). The achieved high efficiency by SnO_2 NG interlayer signifies an important approach to further elevate QDSSCs performance to the next level.

2. Experimental section

2.1. Materials

Tin chloride dihydrate ($SnCl_2 \cdot 2H_2O$), hexamethylenetetramine (HMTA, $C_6H_{12}N_4$), cadmium acetate dihydrate ($Cd(CH_3COO)_2 \cdot 2H_2O$), sodium sulfide ($Na_2S$), sulfur (S) and potassium chloride (KCl) were obtained from Sigma-Aldrich Co., South Korea and used as such without purification. TiO_2 paste (Ti-nanoxide HT/SP) was supplied by Solaronix.

2.2. Preparation of TiO_2/SnO_2 NG/CdS photoelectrode

Prior to the deposition, the fluorine-doped tin oxide (FTO, 13 Ω sq^{-2}) glasses (1.3 × 1.5 cm^2) were well washed with acetone, ethanol and deionized (DI) water for 10 min each. Mesoporous TiO_2 electrodes were prepared using doctor-blading a TiO_2 paste (20 nm diameter, Solaronix SA) onto FTO substrate and then the samples were maintained at 450 °C for 30 min. Then, SnO_2 NG was grown on the TiO_2 surface *via* a facile CBD reaction. In detail, 0.05 M $SnCl_2 \cdot 2H_2O$ and 0.15 M HMTA were mixed in 70 mL DI water under magnetic stirring for 30 min. The as-prepared TiO_2 samples were dipped horizontally into the SnO_2 growth solution and heated at 95 °C for 10 h. The HMTA in precursor solution not only serves as a surfactant by reducing the surface tension between the growth solution and substrate, but also it supports the growth of SnO_2 layer. After deposition, the SnO_2 NG loaded FTO/TiO_2 films were rinsed with DI water and ethanol, and then heated at 450 °C for 30 min. The as-fabricated electrodes are termed the TiO_2/SnO_2 NG.

Next, the CdS QDs were loaded on TiO_2/SnO_2 NG by a facile successive ionic layer adsorption and reaction (SILAR) method. Briefly, TiO_2/SnO_2 NG films were dipped in aqueous 0.1 M $Cd(CH_3COO)_2 \cdot 2H_2O$ solution for 5 min, rinsed with ethanol; then dipped in aqueous 0.1 M Na_2S solution for 5 min, and then once again rinsed with ethanol. Such a process is called one SILAR cycle and a totally 8 SILAR cycles were repeated. The as-obtained films are termed the TiO_2/SnO_2 NG/CdS. The schematic of the fabrication process of TiO_2/SnO_2 NG/CdS on FTO substrate is shown in Fig. 1.

2.3. Counter electrode and QDSSC device fabrication

CuS counter electrodes were prepared on FTO substrates using CBD method following our previous report.[19] Finally, the QDSSCs were sandwiched with as-fabricated TiO_2/SnO_2 NG/CdS photoelectrodes and CuS counter electrodes by a sealant (SX 1170-60, Solaronix) and polysulfide electrolyte containing of 1 M Na_2S, 2 M S and 0.1 M KCl in methanol and water solution (7 : 3).

2.4. Characterization and measurements

The crystalline phase, elemental analysis and morphology of the electrodes were investigated using X-ray diffraction (XRD, D/Max-2400), X-ray photon spectroscopy (XPS, VG Scientific ESCALAB 250) and scanning electron microscope (SEM, S-2400, Hitachi) with energy-dispersive X-ray spectroscopy (EDX, 15 kV) mapping characterizations, respectively. The optical absorption properties of the as-prepared electrodes were analyzed by UV-visible absorption spectra (OPTIZEN 3220UV). The photocurrent–voltage (*J*–*V*) measurements were conducted by an ABET Technologies (USA) solar simulator, which can exhibit an

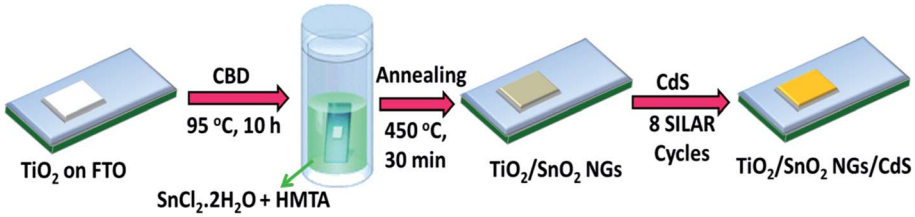

Fig. 1 The schematic of the preparation process of TiO_2/SnO_2 NG/CdS on FTO substrate.

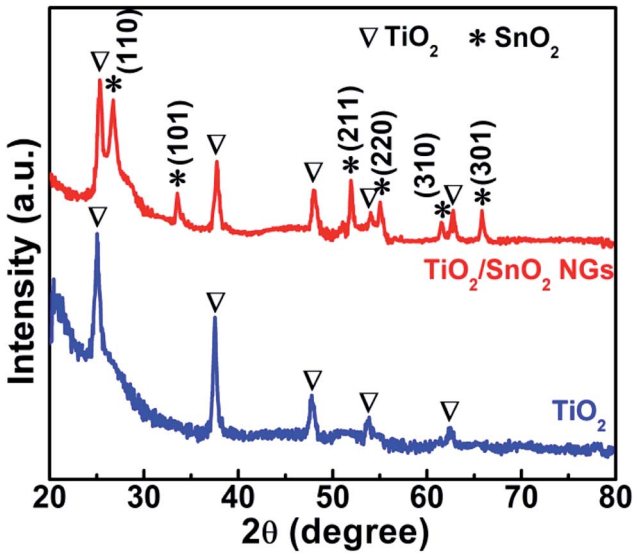

Fig. 2 XRD patterns of TiO_2 and TiO_2/SnO_2 NG on FTO substrate.

intensity of 100 mW cm^{-2}. Electrochemical impedance spectroscopy (EIS) was carried out by a SP-150 BioLogic station with a frequency range of 500 kHz to 0.1 Hz and AC amplitude of 10 mV.

3. Results and discussion

3.1. Structural and morphological characterization

Facile and cost-effective CBD method was used to grow the SnO_2 NG interlayer onto the TiO_2 surface. Initially, the crystalline structure of the TiO_2 and TiO_2/SnO_2 NG electrodes was investigated using XRD characterization. The XRD patterns of the as-prepared TiO_2 and TiO_2/SnO_2 NG are depicted in Fig. 2. As seen in Fig. 2, both the TiO_2 and TiO_2/SnO_2 NG samples exhibit peaks at $2\theta = 25.1°$, $37.5°$, $47.8°$, $53.9°$ and $62.3°$, which are well-matched with the TiO_2 tetragonal anatase structure (JCPDS: 21-1272). After the deposition of SnO_2 over TiO_2 surface, new diffraction peaks are observed at $2\theta = 26.7°$, $33.6°$, $51.9°$, $54.9°$, $61.5°$ and $65.8°$, which are well-consistent with the SnO_2 tetragonal structure (JCPDS: 41-1445).[20]

XPS characterization was performed to investigate the valence states of elements in TiO_2/SnO_2 NG electrode. The XPS survey spectra of TiO_2/SnO_2 NG sample is shown in Fig. 3a, which clearly shows the presence of only Ti, Sn, O and C elements. The presence of carbon element in the total survey scan spectrum is ascribed to the exposure of air sample to air. As depicted in Fig. 3b, the XPS spectrum of Ti 2p, exhibits the Ti $2p_{3/2}$ and Ti $2p_{1/2}$ peaks that are centered at 458.7 and 464.5 eV, respectively. These spectra are consistent with the presence of Ti^{4+} valence state. Due to the spin–orbit

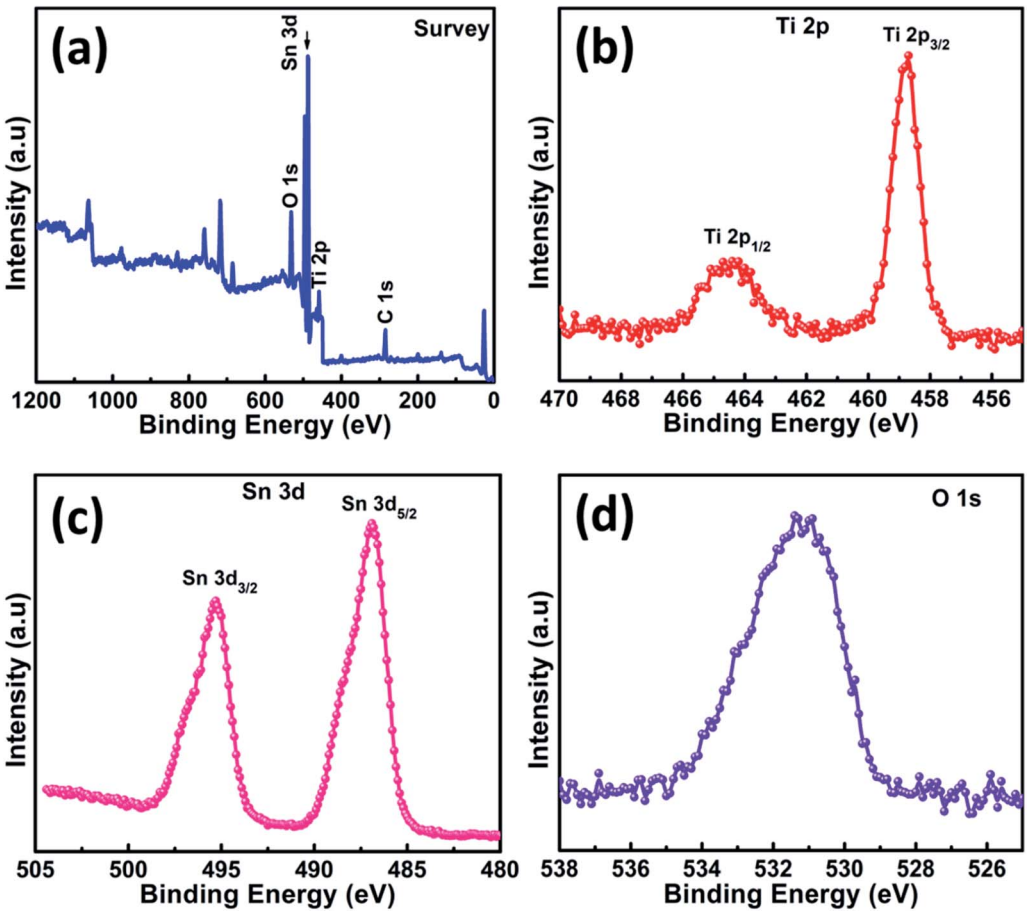

Fig. 3 (a) XPS survey spectra and high-resolution XPS spectra of (b) Ti 2p, (c) Sn 3d and (d) O 1s in TiO_2/SnO_2 NG sample.

coupling of Ti 2p, the obtained peaks are separated by 5.8 eV.[21] The Sn 3d spectrum presented in Fig. 3c exhibited two peaks at 486.8 eV and 495.3 eV which are indexed to Sn $3d_{5/2}$ and Sn $3d_{3/2}$, respectively, and agree with the Sn^{4+} state in SnO_2.[22] As depicted in Fig. 3d, the spectrum of O 1s displays a peak that is centered at 530.9 eV, corresponding to O_2 in the TiO_2 and SnO_2 crystal lattices.[22,23] The XRD and XPS results confirmed the formation of SnO_2 NG on the TiO_2 surface.

The surface morphologies of the as-prepared TiO_2 and TiO_2/SnO_2 NG electrodes were studied by SEM analysis, and the corresponding images are depicted in Fig. 3a and b for TiO_2 on FTO substrate, and in Fig. 4c and d for SnO_2 onto the TiO_2 surface (TiO_2/SnO_2) NG. As shown in Fig. 4a, the TiO_2 nanoparticles are uniformly distributed throughout the substrate. It can be clearly seen from Fig. 4b, that the TiO_2 exhibits spherical nanoparticle morphology with diameter in the range of ~16 to ~20 nm. CBD method was used to grow the SnO_2 nanostructures on the surface of TiO_2. It can be clearly observed in Fig. 4c, that the SnO_2 exhibits the nanograss (NG) morphology. The diameter of the SnO_2 NG was estimated to be in the range of ~21 to ~46 nm (Fig. 4d). The SEM images clearly reveal that the SnO_2 NG nanostructures were successfully grown on TiO_2 surface. In addition, SEM-EDX color mapping was carried out to examine the distribution of elements in the TiO_2/SnO_2 NG. The mapping images shown in Fig. S1† clearly revealed the homogeneous distribution of Ti, Sn and O elements in the as-prepared TiO_2/SnO_2 NG electrode.

3.2. Optical properties

UV-vis absorption measurements were carried out to demonstrate the optical properties of the TiO_2, TiO_2/SnO_2 NG, TiO_2/CdS and TiO_2/SnO_2 NG/CdS samples and the results are plotted in Fig. 5 in the rage of 300 to 800 nm. The TiO_2 sample exhibits the absorption edge at around 378 nm. The growth of SnO_2 NG on TiO_2 surface increased the absorption intensity. In addition, the absorption onset of TiO_2/SnO_2 NG increased to 388 nm. The

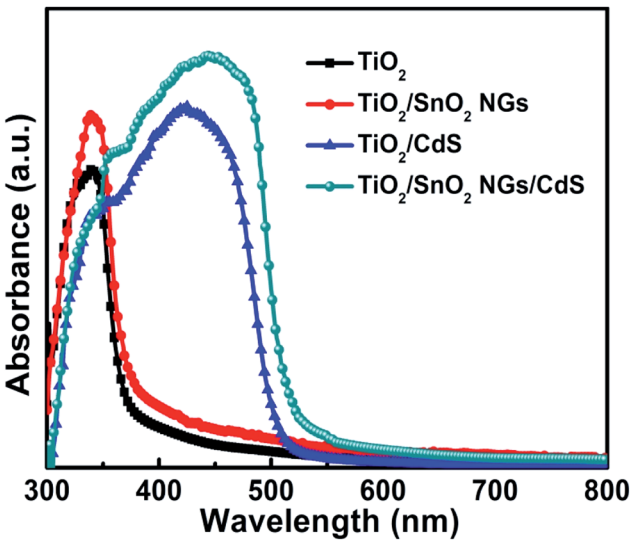

Fig. 5 UV-vis absorption spectra of as-prepared electrodes.

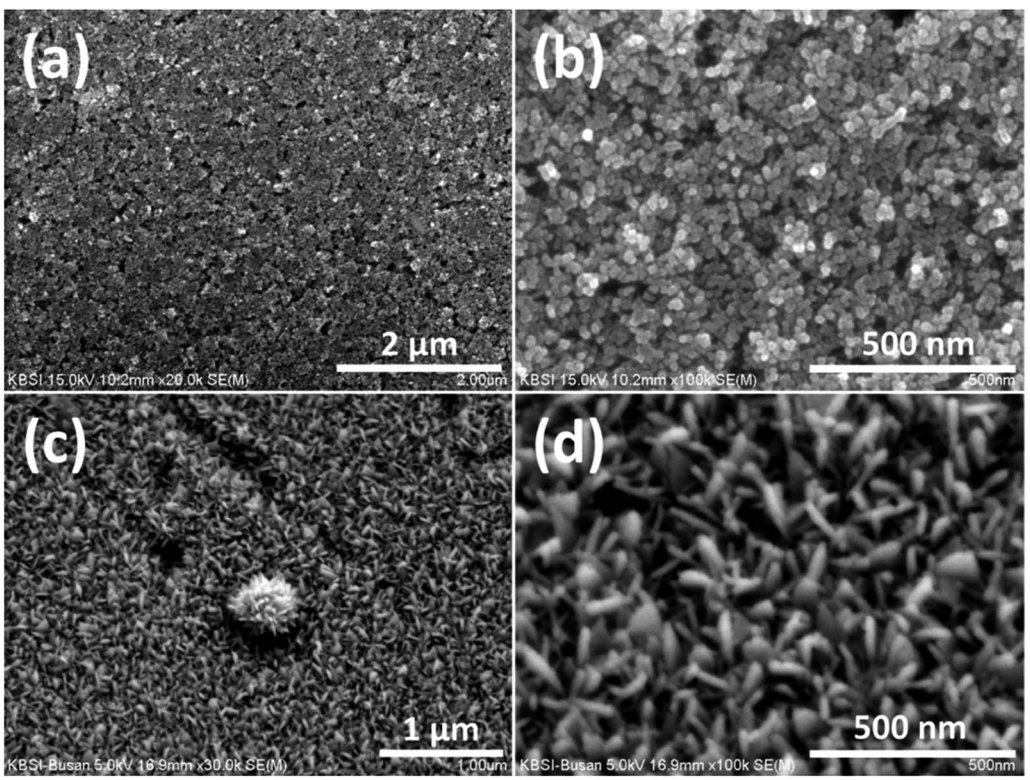

Fig. 4 SEM images of (a and b) TiO_2 and (c and d) TiO_2/SnO_2 NG on FTO substrate at different magnifications.

absorption onsets of the TiO_2/CdS and TiO_2/SnO_2 NG/CdS samples were measured to be 510 nm and 525 nm, respectively. The absorption onset of the TiO_2/SnO_2 NG/CdS electrode was increased and with higher absorbance compared to TiO_2/CdS. These observations can be attributed to the growth of SnO_2 NG passivation/barrier layer over TiO_2 surface. Also, the SnO_2 NG interlayer supports the nucleation and growth of CdS QDs, which results in the high rate absorption of TiO_2/SnO_2 NG/CdS electrode.

3.3. Photovoltaic performance and charge transfer of the QDSSCs

To evaluate the impact of the SnO_2 NG interlayer on the photoanodes, the photovoltaic behaviors of TiO_2/CdS and TiO_2/SnO_2 NG/CdS based QDSSCs have been investigated. The *J–V* profiles of the as-fabricated QDSSCs were measured under one sun illumination and the related photovoltaic considerations are depicted in Fig. 6a and Table 1. The TiO_2/CdS QDSSC exhibits J_{SC} of 6.64 mA cm^{-2}, V_{OC} of 0.614 V, and FF of 0.530, resulting in a PCE of 2.16%. When a SnO_2 NG layer was grown on TiO_2 surface (TiO_2/SnO_2 NG/CdS), the J_{SC}, V_{OC} and FF were considerably improved to 8.92 mA cm^{-2}, 0.619 V, and 0.570, respectively, resulting in the elevated PCE of 3.15%, which is much higher than the PCE of TiO_2/CdS (2.16%) photoelectrode. The enhanced V_{OC} and J_{SC} of the TiO_2/SnO_2 NG/CdS based QDSSCs are attributed to the reduced charge recombination and the fast charge transfer at the TiO_2/QDs/electrolyte interfaces. Hence, the PCE of QDSSC has improved from 2.16% to 3.15% by the growth of SnO_2 NG interlayer over the TiO_2 surface. Furthermore, incident photon to current conversion efficiency (IPCE) study was carried out to illustrate the light absorption and electron generation behaviors in the QDSSCs. Fig. 6b depicts the IPCE plots of the as-prepared QDSSCs. It is evident from the IPCE spectra that the introduction of SnO_2 NG interlayer enhanced the IPCE response from 66% to 75% and also enlarged the IPCE response edge from 548 nm to 568 nm. The TiO_2/SnO_2 NG/CdS based QDSSCs exhibits higher IPCE response than the TiO_2/CdS, which is in good agreement with the J_{SC} of the *J–V* plots.

In order to demonstrate the impact of SnO_2 NG interlayer on the photoelectrode films, EIS measurement was conducted under forward bias (V_{OC}) and illumination. The Nyquist plots of the TiO_2/CdS and TiO_2/SnO_2 NG/CdS based QDSSCs are depicted in Fig. 6c. The Nyquist plots of both devices exhibit the two semicircles, in which the first (small) semicircle is obtained in the high-frequency region and represents the charge transfer resistance (R_{CE}), the chemical capacitance (C_{CE}) at the interface of the counter electrode/electrolyte, and the series resistance (R_S) which is obtained in the high-frequency region where the

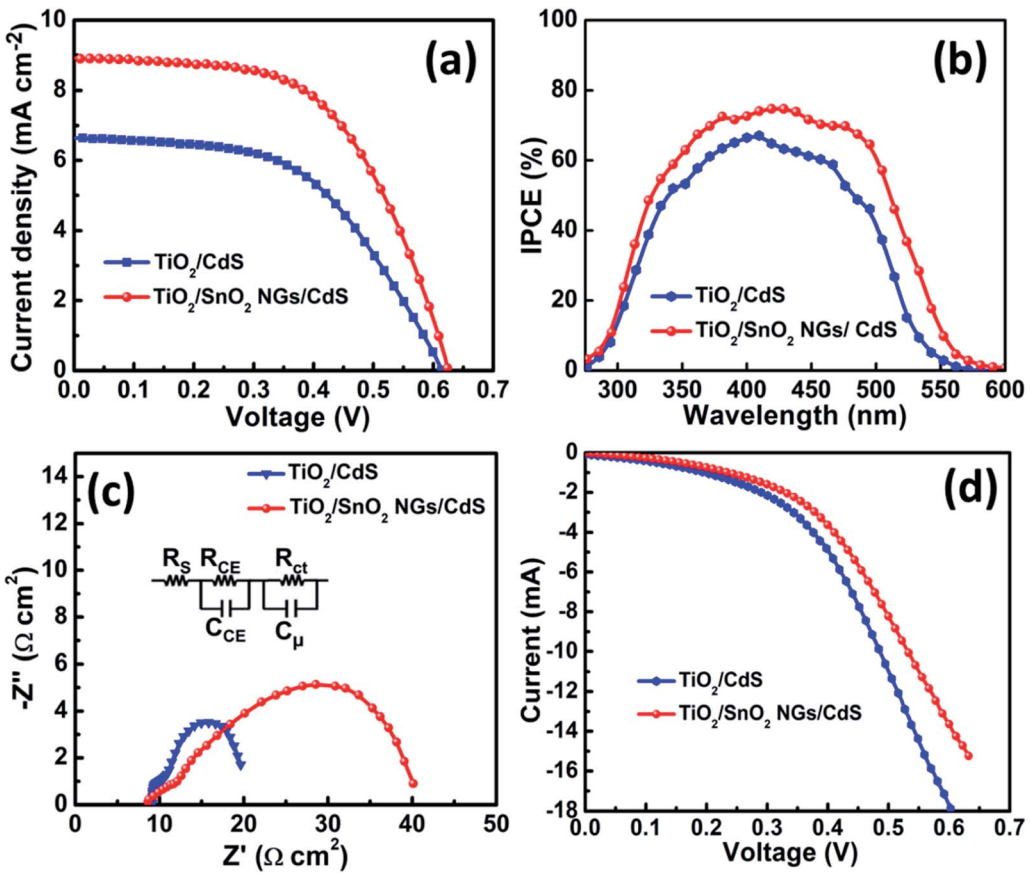

Fig. 6 (a) *J–V*, (b) IPCE and (c) EIS profiles of QDSSCs based on TiO_2/CdS and TiO_2/SnO_2 NG/CdS photoelectrodes. (d) *J–V* profiles of QDSSCs under dark current.

Table 1 Photovoltaic parameters of the as-prepared QDSSCs based on TiO_2/CdS and TiO_2/SnO_2 NG/CdS photoelectrodes under one sun illumination

Cell	V_{OC} (V)	J_{SC} (mA cm^{-2})	FF	PCE%	R_{ct} (Ω)	C_μ (μm)	τ_e (ms)
TiO_2/CdS	0.614	6.64	0.530	2.16	8.78	1358	11.92
TiO_2/SnO_2 NG/CdS	0.619	8.92	0.570	3.15	27.94	2183	60.99

phase is zero. The recombination resistance (R_{ct}) at the TiO_2/QD/electrolyte interface and the chemical capacitance (C_μ) indexed to the bigger semicircle which is obtained at mid/low frequency.[24,25] Based on the equivalent circuit model (inset of Fig. 6c) and using Z-view software, the Nyquist plots were fitted to obtain the R_{ct} values and the fitting results are summarized in Table 1. There is no considerable change in the R_{CE}, which is due to the usage of similar electrolyte and counter electrode in the fabrication of QDSSCs. However, R_{ct} of the TiO_2/SnO_2 NG/CdS based QDSSC (27.94 Ω cm^2) is much higher than that of the TiO_2/CdS (8.78 Ω cm^2). The higher R_{ct} of the TiO_2/SnO_2 NG/CdS based QDSSC demonstrates that the growth of SnO_2 NG over the TiO_2 surface successfully suppresses the electron recombination at the TiO_2/QDs/electrolyte interfaces.[24] Hence, the growth of SnO_2 NG interlayer hinders the interfacial charge recombination and enhances the photovoltaic performance (J_{SC} and FF). Moreover, QDSSC based on TiO_2/SnO_2 NG/CdS photoelectrode achieves higher C_μ (2183 μF) than that of the TiO_2/CdS (1358 μF) system. The higher C_μ of the TiO_2/SnO_2 NG/CdS system demonstrates the improved collection of photo-excited electrons into the conduction band of photoanode, which is mainly due to the hindered recombination at the TiO_2/QDs/electrolyte interfaces. Further, the electron life time (τ_e) of the QDSSCs can be obtained using the following equation,[26]

$$\tau_e = R_{ct} \times C_\mu \quad (1)$$

Interestingly, the τ_e of the TiO_2/CdS with SnO_2 NG interlayer (60.99 ms) is much higher than that of the SnO_2 NG-free device (11.92 ms), which reveals the higher charge collection efficiency of the TiO_2/SnO_2 NG/CdS system.

Under the dark condition, the *J–V* plots of the TiO_2/CdS and TiO_2/SnO_2 NG/CdS based QDSSCs were obtained and are shown in Fig. 6d. The electron recombination occurs at the interfaces of TiO_2/QDs and TiO_2/electrolyte, and this is the source of dark current.[27] Hence, a dark current study is a useful indicator of charge recombination. With the introduction of SnO_2 NG interlayer, the TiO_2/SnO_2 NG/CdS device delivers the reduced dark current, which is lower compared with that of the TiO_2/CdS device. The reduction of the dark current arose from an enhancement in electron transport with decreasing the internal resistance. As a result, the electron recombination was effectively reduced by the introduction of the SnO_2 NG interlayer, and this contributed to the enhanced current and decreased electron loss.

Furthermore, to investigate the impact of SnO_2 NG interlayer on the performance of QDSSCs, EIS tests were conducted at various bias applied voltages under dark condition in the 500 kHz to 100 mHz frequency range. The obtained recombination resistance (R_{rec}) and chemical capacitance (C_μ) from the corresponding EIS tests are depicted in Fig. 7a and b, respectively. The R_{rec} and C_μ reveal that the charge recombination process occurs at the TiO_2/QDs/electrolyte interfaces. A higher R_{rec} represents the low recombination rate and grater C_μ values denote the Fermi level upward shift, yielding the enhanced V_{OC}.[16] It can be seen from Fig. 6a that the R_{rec} values of both devices decrease with the increment of the forward bias voltage due to the increased Fermi level of TiO_2 at the forward bias. Also, TiO_2/SnO_2 NG/CdS QDSSCs exhibits higher R_{rec} values than the TiO_2/CdS device under identical bias voltages. The recombination rate is inversely proportional R_{rec}.[13] Moreover, the higher C_μ values of the TiO_2/SnO_2 NG/CdS device denote the

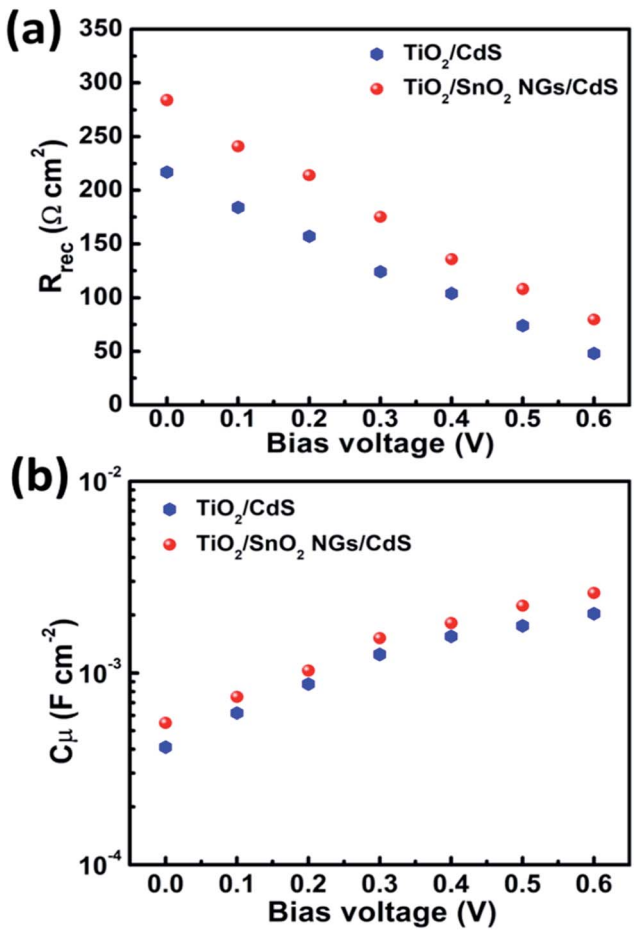

Fig. 7 EIS (a) recombination resistance (R_{rec}) and (b) chemical capacitance (C_μ) at various forward bias voltages (V).

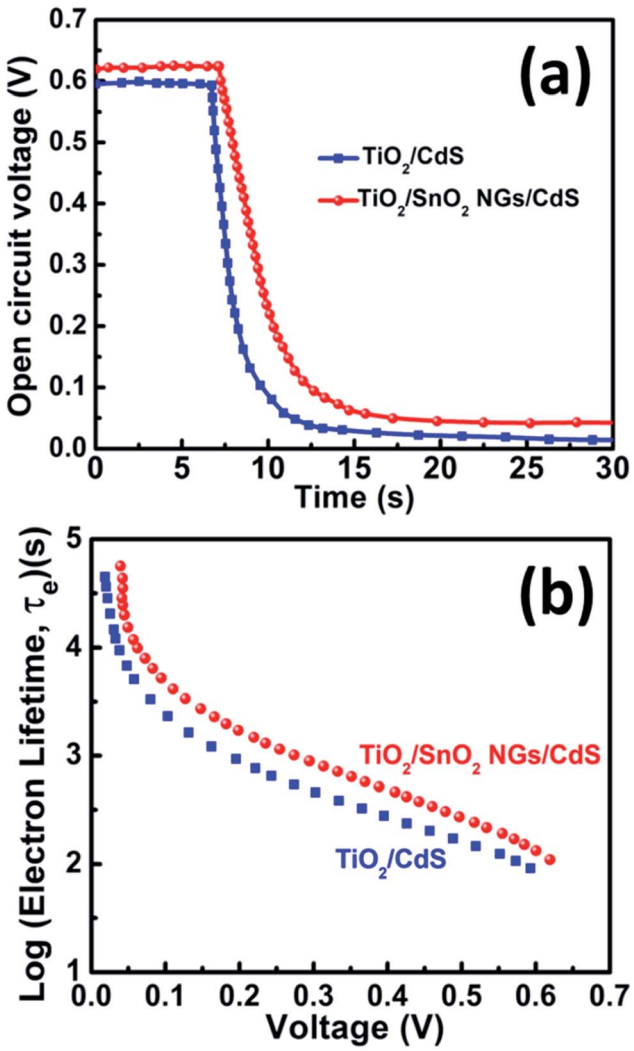

Fig. 8 (a) V_{OC} decay profiles of TiO_2/CdS and TiO_2/SnO_2 NG/CdS QDSSCs. (b) Electron life time (in log-linear notation) obtained from V_{OC} decay measurements.

upward shift of the Fermi level of TiO_2, resulting in large V_{OC}. These EIS studies reveal the reduced recombination rate for the TiO_2/SnO_2 NG/CdS device, which is favorable for the improved J_{SC} and FF.

The excited electrons life time was examined using the open-circuit voltage (V_{OC}) decay studies with time. Initially, the QDSSCs were irradiated with one sun illumination to a steady voltage, then the illumination was turned off and the V_{OC} decay data was obtained. Fig. 8a depicts the V_{OC} decay profiles of the TiO_2/CdS and TiO_2/SnO_2 NG/CdS based QDSSCs. The V_{OC} decay plots clearly exhibit the continued monitoring of V_{OC} values under illumination and approach to decay after switching off the illumination. It is evident from the V_{OC} decay plots that the TiO_2/SnO_2 NG/CdS based QDSSCs exhibit a slower voltage decay rate than the TiO_2/CdS photoanode. This behavior is mainly attributed to the SnO_2 NG interlayer which efficiently suppresses the charge recombination at the TiO_2/QDs/electrolyte interfaces and also promotes the efficient electron transfer. Further, the electron life time (τ_e) can be estimated using the following equation:[28]

$$\tau_e = -\left(\frac{k_B T}{e}\right)\left(\frac{dV_{OC}}{dt}\right)^{-1} \quad (2)$$

where, k_B, T and e have their usual meanings. Fig. 8b displays the plot of electron life time (τ_e, in log sign) as a function of V_{OC}.[29] The TiO_2/SnO_2 NG/CdS based QDSSCs deliver longer τ_e values than that of TiO_2/CdS, implying a suppressed recombination of the photo-generated electrons leading to the efficient charge transfer, which agrees well with the EIS analysis.

Fig. 9 depicts the impact of the SnO_2 NG interlayer on the charge transfer mechanism in QDSSCs. As shown in Fig. 9a, upon illumination, CdS captures the photons and produces the electron–hole pairs, named excitons. Then the electrons transfer into TiO_2 conduction band, while the holes are reduced by polysulfide electrolyte. Simultaneously, the possibility of charge recombination also takes place at the interfaces of TiO_2/CdS QDs/electrolyte, which results in poor photovoltaic performance (Fig. 9a). Hence, SnO_2 NG interlayer was introduced between the

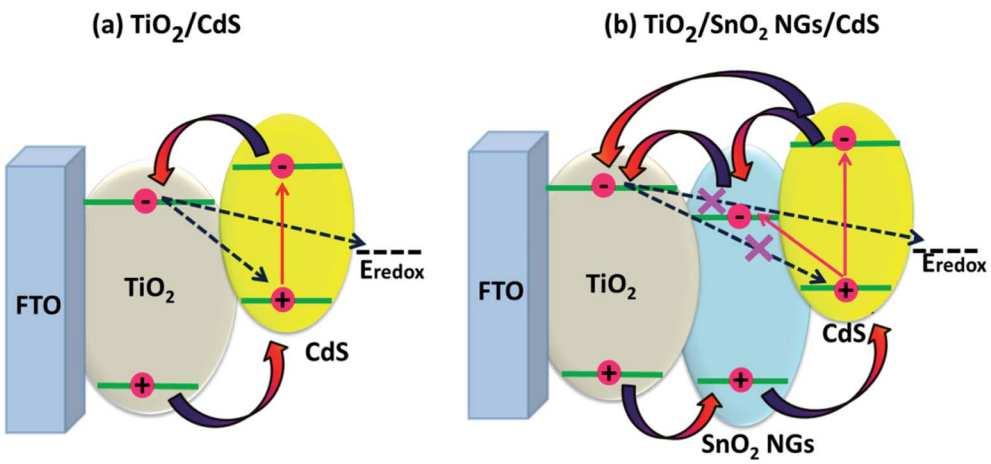

Fig. 9 Schematic demonstration of the charge transfer pathways in (a) TiO_2/CdS and (b) TiO_2/SnO_2 NG/CdS based QDSSCs.

TiO_2 and CdS QDs (TiO_2/SnO_2 NG/CdS) to prevent the charge recombination (Fig. 9b). The introduction of SnO_2 NG interlayer on TiO_2 surface retards the back injection of the electron from TiO_2 to QDs and also prevents the injection of excited electron from TiO_2 to redox couple, resulting in the high photovoltaic performance. Therefore, introducing SnO_2 NG interlayer over the TiO_2 surface achieves the outstanding properties, such as wide solar light-harvesting ability, enhanced charge transfer and suppressed charge recombination at the TiO_2/QDs/electrolyte interfaces.

4. Conclusions

In summary, the introduction of SnO_2 NG layer between the TiO_2 and CdS QDs achieved the higher light-harvesting ability, improved charge transport and suppressed charge recombination at the TiO_2/QDs/electrolyte interfaces. Evident from the *J–V*, EIS, IPCE, V_{OC} decay and dark current measurements indicate that the photovoltaic properties of the TiO_2/CdS QDSSCs were drastically enhanced after the deposition of SnO_2 NG layer due to the improved light absorption, fast charge transfer, reduced charge recombination and prolonged electron life time. Hence, the introduction of SnO_2 NG interlayer could be a favorable and effective approach to considerably improve the performance of QDSSCs. As a result, TiO_2/SnO_2 NG/CdS based QDSSCs achieved the PCE (3.15%), V_{OC} (0.619 V), J_{SC} (8.92 mA cm^{-2}), and FF (0.570), respectively, which are superior to TiO_2/CdS device (PCE = 2.16%, V_{OC} = 0.614 V, J_{SC} = 6.64 mA cm^{-2}, and FF = 0.530).

Conflicts of interest

The authors declare no competing financial interest.

Acknowledgements

This work was supported by UAEU Program for Advanced Research (UPAR) under grant no. 31S312. Also, this work was supported by BK 21 PLUS, Creative Human Resource Development Program for IT Convergence, Pusan National University, Busan, South Korea.

References

1 W. Li and X. Zhong, *J. Phys. Chem. Lett.*, 2015, **6**, 796–806.
2 A. J. Nozik, M. C. Beard, J. M. Luther, M. Law, R. J. Ellingson and J. C. Johnson, *Chem. Rev.*, 2010, **110**, 6873–6890.
3 M. Ye, X. Gao, X. Hong, Q. Liu, C. He, X. Liu and C. Lin, *Sustainable Energy Fuels*, 2017, **1**, 1217–1231.
4 Z. Y. Yang, J. Z. Fan, A. H. Proppe, F. P. Arquer, D. Rossouw, O. Voznyy, X. Z. Lan, M. Liu, G. Walters, R. Q. Bermudez, B. Sun, S. Hoogland, G. A. Botton, S. O. Kelley and E. H. Sargent, *Nat. Commun.*, 2017, **8**, 1325.
5 R. L. Wu, T. Y. Wang, M. Wu, Y. B. Lv, X. P. Liu, J. J. Li, H. B. Shen and L. S. Li, *Chem. Eng. J.*, 2018, **348**, 447–454.
6 H. J. Kim, S. W. Kim, C. V. V. M. Gopi, S. K. Kim, S. S. Rao and M. S. Jeong, *J. Power Sources*, 2014, **268**, 163–170.
7 M. P. A. Muthalif, C. D. Sunesh and Y. Choe, *Appl. Surf. Sci.*, 2018, **440**, 1022–1026.
8 P. Subramanyam, P. Ghosal, M. Deepa and C. Subrahmanyam, *Electrochim. Acta*, 2018, **278**, 374–384.
9 W. Wang, W. L. Feng, J. Du, W. N. Xue, L. L. Zhang, L. L. Zhao, Y. Li and X. H. Zhong, *Adv. Mater.*, 2018, **30**, 1705746.
10 C. V. V. M. Gopi, M. V. Haritha, S. K. Kim and H. J. Kim, *Nanoscale*, 2015, **7**, 12552–12563.
11 F. Huang, Q. Zhang, B. Xu, J. Hou, Y. Wang, R. C. Masse, S. Peng, J. Liu and G. Cao, *J. Mater. Chem.*, 2016, **4**, 14773–14780.
12 C. V. V. M. Gopi, M. V. Haritha, H. Seo, S. Singh, S. K. Kim, M. Shiratani and H. J. Kim, *Dalton Trans.*, 2016, **45**, 8447–8457.
13 Z. Ren, J. Wang, Z. Pan, K. Zhao, H. Zhang, Y. Li, Y. Zhao, I. M. Sero, J. Bisquert and X. Zhong, *Chem. Mater.*, 2015, **27**, 8398–8405.
14 J. M. Li, *CrystEngComm*, 2017, **19**, 32–39.
15 Y. S. Lee, C. V. V. M. Gopi, M. V. Haritha and H. J. Kim, *Dalton Trans.*, 2016, **45**, 12914–12923.
16 Z. Du, H. Zhang, H. Bao and X. Zhong, *J. Mater. Chem. A*, 2014, **2**, 13033–13040.
17 S. Ozu, Y. Zhang, H. Yasuda, Y. Kitabatake, T. Toyoda, M. Hirata, K. Yoshino, K. Katayama, S. Hayase and R. Wang, *Front. Energy Res.*, 2019, **7**, 11.
18 E. N. Jayaweera, G. R. A. Kumara, C. Kumarage, S. K. Ranasinghe, R. M. G. Rajapakse, H. M. N. Bandara, O. A. Ileperuma and B. S. Dassanayake, *J. Photochem. Photobiol., A*, 2018, **364**, 109–115.
19 C. V. V. M. Gopi, M. V. Haritha, S. K. Kim, S. S. Rao, D. Punnoose and H. J. Kim, *RSC Adv.*, 2015, **5**, 2963–2967.
20 G. E. Patil, D. D. Kajale, V. B. Gaikwad and G. H. Jain, *Int. Nano Lett.*, 2012, **2**, 1–5.
21 A. Ray, A. Roy, P. Sadhukhan, S. R. Chowdhury, P. Maji, S. K. Bhattachrya and S. Das, *Appl. Surf. Sci.*, 2018, **443**, 581–591.
22 D. Wang, M. Zhang, Z. Chen, H. Li, A. Chen, X. Wang and J. Yang, *Sens. Actuators, B*, 2017, **250**, 533–542.
23 A. Hodaei, A. S. Dezfuli and H. R. Naderi, *J. Mater. Sci.: Mater. Electron.*, 2018, **29**, 14596–14604.
24 F. Huang, J. Hou, Q. Zhang, Y. Wang, R. C. Massé, S. L. Peng, H. L. Wang, J. S. Liu and G. Z. Cao, *Nano Energy*, 2016, **26**, 114–122.
25 R. Zhou, Q. F. Zhang, E. Uchaker, J. Lan, M. Yin and G. Z. Cao, *J. Mater. Chem. A*, 2014, **2**, 2517–2525.
26 H. Kim, G. Xu, C. V. V. M. Gopi, H. Seo, M. V. Haritha and M. Shiratani, *J. Electroanal. Chem.*, 2017, **788**, 131–136.
27 J. Bisquert, A. Zaban, M. Greenshtein and I. M. Seró, *J. Am. Chem. Soc.*, 2004, **126**, 13550–13559.
28 S. B. Ambade, R. B. Ambade, R. S. Mane, G. W. Lee, S. F. Shaikh, S. A. Patil, O. S. Joo, S. H. Han and S. H. Lee, *Chem. Commun.*, 2013, **49**, 2921–2923.
29 H. Seo, D. Ichida, S. Hashimoto, N. Itagaki, K. Koga, M. Shiratani, S. H. Nam and J. H. Boo, *J. Nanosci. Nanotechnol.*, 2016, **16**, 4875–4879.

